Supplementary Information for:
Accelerating the design of photocatalytic surfaces for antimicrobial application: machine learning based on a sparse dataset

Heesoo Park, El Tayeb Bentria, Sami Rtimi*, Abdelilah Arredouani,
Halima Bensmail, and Fedwa El Mellouhi**

*Sami Rtimi
E-mail: rtimi.sami@gmail.com
and
**Fedwa El Mellouhi
E-mail: felmellouhi@hbku.edu.qa

Mechanism of photocatalytic hydrogen peroxide production

Because of its favorable characteristics, including low toxicity and thermodynamic and electrochemical stability in aqueous media, TiO_2 is one of the most intensively studied semiconducting photocatalysts. In addition, loading TiO_2 with co-catalysts of noble metals such as Pd, Pt, Au, and Ag improves TiO_2's photoinduced catalytic reaction by increasing its catalytic reactivity. These characteristics enable the tailoring of the system's catalytic properties towards the desired results. The loading with noble metals modifies the physicochemical properties, and if properly designed, the photo-generated electrons from TiO_2 are transported towards the interfaces where other materials' properties such as band edge positions and adsorption enthalpies need to be optimized [1].

While the combination of semiconductors with co-catalysts is a widely used approach to promote the performance of photocatalysts, the chemical activities of metal–TiO_2 depend on various chemical and physical parameters. For example, during the metallic nanoparticle deposition, the chemical condition controls the metal dispersion on the semiconductor, in terms of the amount of loaded metal [2], and the surface and interface properties [3]. In such hybrid photocatalytic structures, co-catalysts themselves are often not the light-harvesting components; they rather play the role of trapping and collecting the photoinduced charge carriers and drive the charge kinetics within the photocatalytic process: i) trapping charge carriers to populate the separated electrons and holes at the equilibrium by forming an interface with semiconductor; and ii) providing highly active reaction sites to transfer the trapped charges to the electrolyte to perform redox reactions [4, 5].

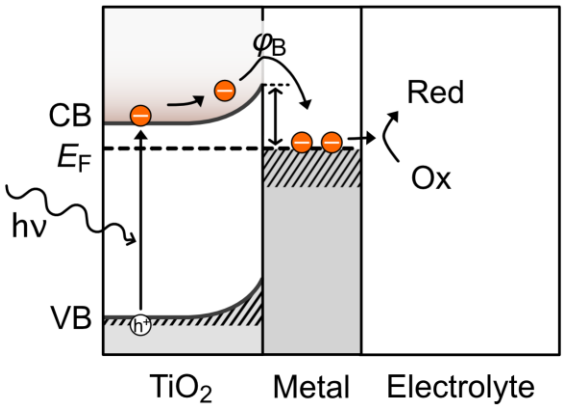

Figure S1: Schematic illustration of band-energy alignments of semiconductor/co-catalyst (TiO_2/ Metal) with the electrolytes. The upward band bending is called the Schottky barrier, φ_B. The Fermi level at the equilibrium is denoted as E_F, and the valence and conduction bands are marked as VB and CB, respectively. Electron and hole pairs are generated at the semiconductor band edges upon illumination.

From a device perspective, the formation of heterojunctions governs the electron transfer that consequently dominates the photocatalytic reaction [6]. The photoexcitation of TiO_2 produces electron–hole (e^-–h^+) pairs. These generated carriers are prone to recombining unless they are separated and transported to the interfaces. The height of the Schottky barrier (φ_B) (see Figure 1), which is characterized by the conduction band (CB) of TiO_2 and the Fermi level at the interface equilibrium, determines the charge carrier population, resulting in efficient e^-–h^+ separation.

Subsequently, redox reactions, such as water splitting, occur on the surface of the noble metal particle. The atomistic configuration on the surface determines the adsorption of the reacting species. At the same time, the redox potential level of electrolyte should be higher than the work function of metal to promote the desired reaction. Therefore, the Fermi level and work function of noble metal co-catalysts are key parameters to tailor the activity and selectivity of the photocatalytic systems.

For example, a photocatalytic system desirable for H_2O_2 generation [7] via the reduction of oxygen and water offers a venue to optimize materials capable of inhibiting infectious microorganisms. While H_2O_2 is formed by two-electron reduction of O_2 and $2H^+$ ($O_2 + 2H^+ + 2e^- \rightarrow H_2O_2$), tuning the properties of the co-catalysts offers the possibility of tailoring the optimal levels of H_2O_2 production and degradation. Recently, Tsukamoto et al. reported H_2O_2 production using anatase TiO_2 loaded with bimetallic Au—Ag co-catalysts [8]. This direct synthesis approach from O_2 is an alternative process from the viewpoint of green chemistry and antimicrobial applications. While they controlled the synthesis process by varying the loading of co-catalyst and Au and Ag composition in the bimetallic nanoparticles, the chemical reaction rates were examined. They reported the rates of H_2O_2 formation (k_f) and decomposition (k_d) obtained from their experiments. They considered pure TiO_2 photocatalysts as the control (baseline) sample data. In this work, we denote a catalyst by separating the co-catalyst loading (NP mol %) and alloy composition ($Au_xAg_{(1-x)}$, where $0 \leq x \leq 1$). As an example of NP mol %

co-catalyst loading compound, $Au_xAg_{(1-x)}/TiO_2$ catalyst consists of $(NP \times x)$ mol % Au and $(NP \times (1-x))$ mol % Ag. Accordingly, for the pure TiO_2 catalyst, $NP \to 0+$.

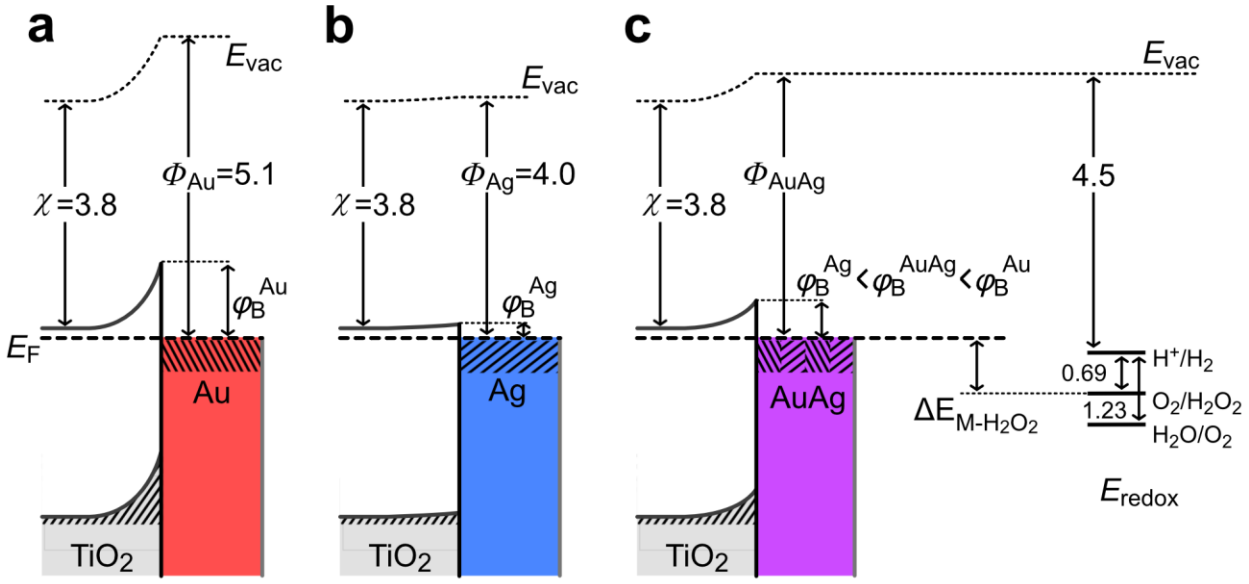

Figure S2: Schematic energy-band diagrams for (a) Au/TiO_2, (b) Ag/TiO_2, and (c) Au_xAg_y / TiO_2 heterojunction. The Schottky barrier height in the Au_xAg_y / TiO_2 heterojunction, Φ_B^{AuAg}, is between Φ_B^{Ag} and Φ_B^{Ag}. We denote the Fermi level, electron affinity of TiO_2, work function of metal, and Schottky barrier of metal as E_F, χ, Φ_M, and Φ_B^M, respectively.

Figure 2 represents the band alignment diagram with the relative heights of the Schottky barrier (φ_B) at equilibrium by varying the composition of Au-Ag nanoparticles. The population of trapped electrons is associated with the net current density passing through the junction. This separated population results from the suppressed recombination of e^-–h^+ in the heterojunction while the rapid recombination of e^-–h^+ occurs due to the low Schottky barrier. This net current can be described as a function of the Schottky barrier [4,9]:

$$J = \left(A^* T^2 \exp\left[\frac{-q \cdot \varphi_B}{k_B T}\right]\right) \cdot \left(\exp\left[\frac{qV_D}{k_B T}\right] - 1\right)$$

where A^* is the effective Richardson constant of the semiconductor for thermionic emission, T is the temperature, q is the elementary charge, k_B is Boltzmann constant, and V_D is the difference of Fermi level between the metal and the semiconductor before the equilibrium.

Considering the relationship between the trapped charge population and energy differences, we prepared the dataset, as described in the following section. While focusing on the population of trapped electrons since the electron occupation distribution follows the Boltzmann statistics for electrons, when the energy difference is much larger than $k_B T$, we could represent the production rate as being consistent with the experiments.

Table S1. Used dataset in the regression models.

Compound	NP's load	[H_2O_2]	k_f	k_d	k_f / k_d	ΔE_{TiO_2-M}	$\Delta E_{M-H_2O_2}$
$Au_{0.1}/TiO_2$	0.1	1.2	0.32	0.26	1.230769231	0.9	0.09
$Au_{0.2}/TiO_2$	0.2	1.5	0.44	0.28	1.571428571	0.9	0.09
$Au_{0.3}/TiO_2$	0.3	1.5	0.51	0.33	1.545454545	0.9	0.09
$Au_{0.4}/TiO_2$	0.4	1.5	0.52	0.33	1.575757576	0.9	0.09
$Au_{0.5}/TiO_2$	0.5	1.4	0.53	0.35	1.514285714	0.9	0.09
$Au_{0.1}Ag_{0.1}/TiO_2$	0.2	1.7	0.42	0.22	1.909090909	0.461115746	0.528884254
$Au_{0.1}Ag_{0.2}/TiO_2$	0.3	2.3	0.47	0.18	2.611111111	0.323380534	0.666619466
$Au_{0.1}Ag_{0.4}/TiO_2$	0.5	3.6	0.57	0.14	4.071428571	0.216128628	0.773871372
$Au_{0.1}Ag_{0.6}/TiO_2$	0.7	1.8	0.32	0.13	2.461538462	0.170945544	0.819054456
$Au_{0.1}Ag_{0.8}/TiO_2$	0.9	1.1	0.16	0.11	1.454545455	0.146043888	0.843956112
$Ag_{0.4}/TiO_2$	0.4	1	0.15	0.12	1.25	0.06	0.93
***$Au_{0.1}Ag_{0.1}/TiO_2$**	0	0.5	0.18	0.34	0.529411765	0.461115746	0.528884254
***$Au_{0.1}Ag_{0.2}/TiO_2$**	0	0.5	0.18	0.34	0.529411765	0.323380534	0.666619466
***$Au_{0.1}Ag_{0.4}/TiO_2$**	0	0.5	0.18	0.34	0.529411765	0.216128628	0.773871372
***$Au_{0.1}Ag_{0.6}/TiO_2$**	0	0.5	0.18	0.34	0.529411765	0.170945544	0.819054456
***$Au_{0.1}Ag_{0.8}/TiO_2$**	0	0.5	0.18	0.34	0.529411765	0.146043888	0.843956112

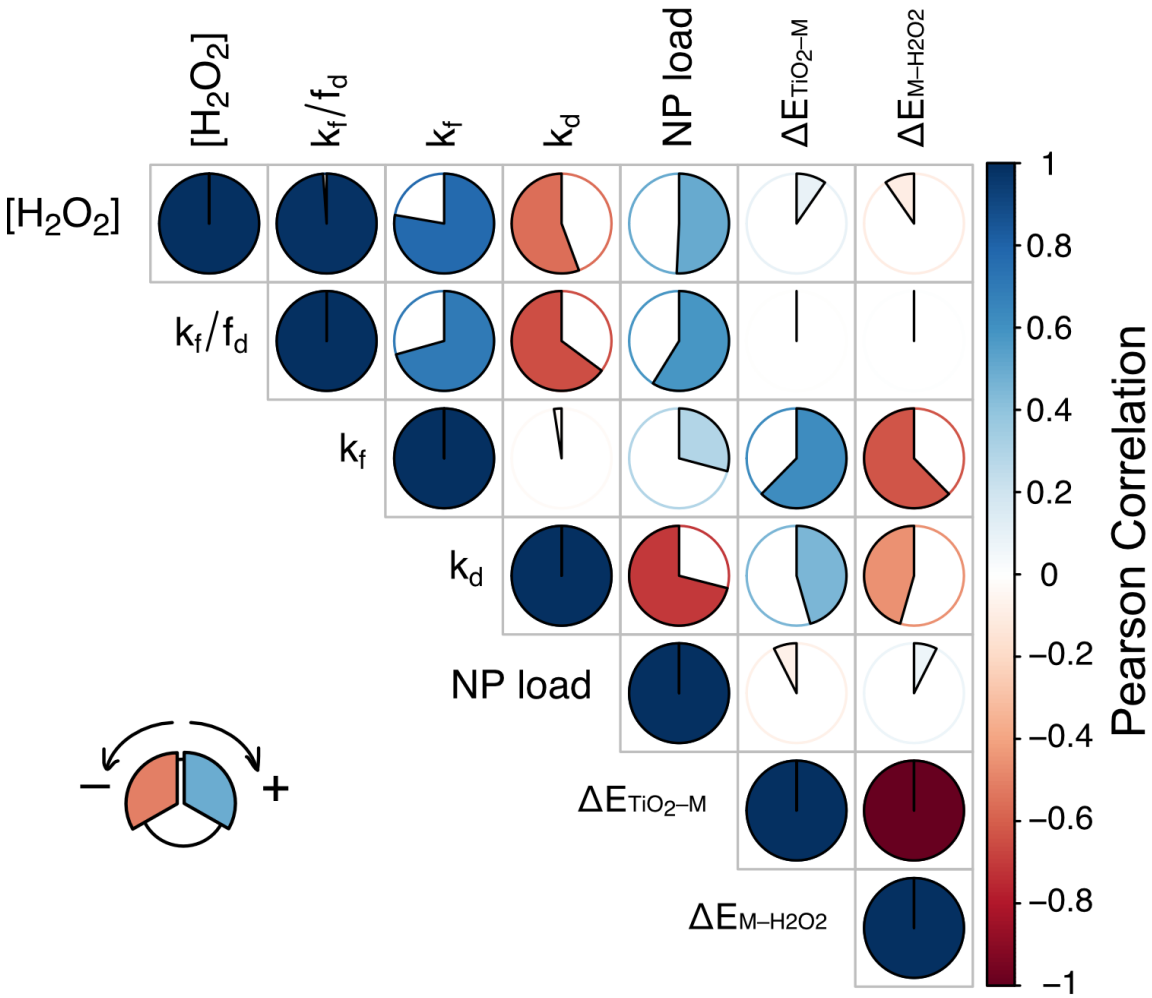

Figure S3: Pearson correlation coefficient between input and target variables for the GAM models built in this work.

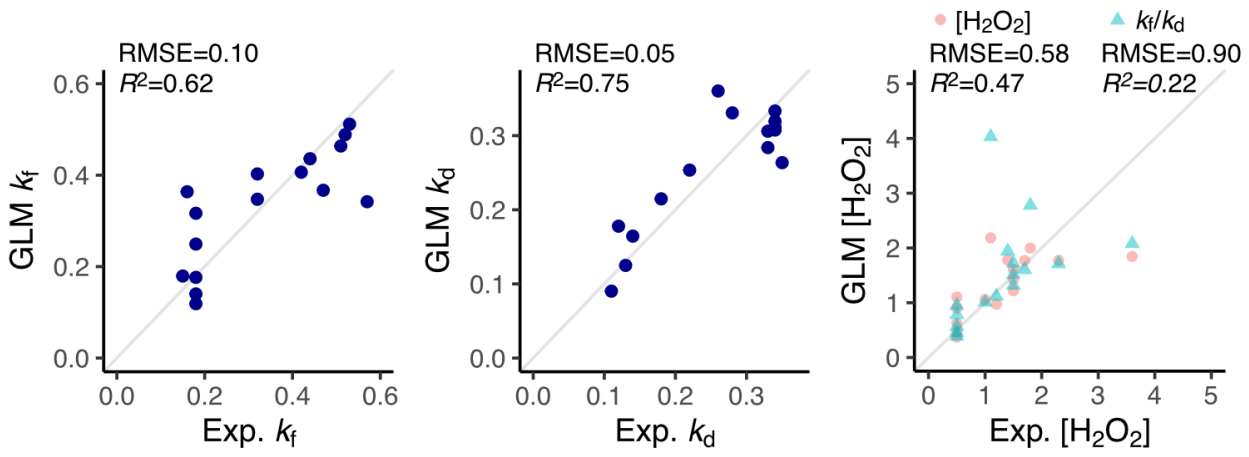

Figure S4: Pair-wise comparison between the experimental and GLM-predicted values for the models (a) k_{f}, (b) k_{d}, and (c) [H_2O_2] and $k_{\mathrm{f}}/k_{\mathrm{d}}$ at t=∞. Meanwhile, the predicted values of k_{f} and k_{d} were used for the calculated $k_{\mathrm{f}}/k_{\mathrm{d}}$ values to be compared with the predicted [H_2O_2] concentration.

References

[1] N. Thomas, D. D. Dionysiou, and S. C. Pillai. Heterogeneous fenton catalysts: A review of recent advances. *Journal of Hazardous Materials*, 404:124082, 2021.

[2] L. Gomathi Devi and R. Kavitha. A review on plasmonic metal□TiO2 composite for generation, trapping, storing and dynamic vectorial transfer of photogenerated electrons across the Schottky junction in a photocatalytic system. *Applied Surface Science*, 360:601–622, 2016.

[3] S. Bai, W. Yin, L. Wang, Z. Li, and Y. Xiong. Surface and interface design in cocatalysts for photocatalytic water splitting and CO2 reduction. *RSC Advances*, 6(62):57446–57463, 2016.

[4] Y. Ma, X. Wang, Y. Jia, X. Chen, H. Han, and C. Li. Titanium dioxide-based nanomaterials for photocatalytic fuel generations. *Chem Rev*, 114(19):9987–10043, 2014.

[5] S. Bai, J. Jiang, Q. Zhang, and Y. Xiong. Steering charge kinetics in photocatalysis: intersection of materials syntheses, characterization techniques and theoretical simulations. *Chem Soc Rev*, 44(10):2893–939, 2015.

[6] Z. Wang, N. Xue, and J. Chen. Semiconductor?□?cocatalyst interfacial electron transfer dominates photocatalytic reaction. *J. Phys. Chem. C*, 123(40):24404–24408, 2019.

[7] H. Tada. Overall water splitting and hydrogen peroxide synthesis by gold nanoparticle-based plasmonic photocatalysts. *Nanoscale Advances*, 1(11):4238–4245, 2019.

[8] D. Tsukamoto, A. Shiro, Y. Shiraishi, Y. Sugano, S. Ichikawa, S. Tanaka, and T. Hirai. Photocatalytic H2O2 production from ethanol/O2 system using TiO2 loaded with Au?□?Ag bimetallic alloy nanoparticles. *ACS Catalysis*, 2(4):599–603, 2012.

[9] M. Ni, M. Leung, D. Leung, and K. Sumathy. Theoretical modeling of TiO2/TCO interfacial effect on dye-sensitized solar cell performance. *Solar Energy Materials and Solar Cells*, 90(13):2000–2009, 2006.